J. Fluid Mech. (1994), *vol.* 271, *pp.* 103–118

Steady and oscillatory bimodal convection

By R. M. CLEVER AND F. H. BUSSE

Institute of Geophysics and Planetary Physics, University of California, Los Angeles, CA 90007, USA *and* Institute of Physics, University of Bayreuth, D-95440 Bayreuth, Germany

(Received 26 July 1993 and in revised form 29 November 1993)

Steady three-dimensional convection in the form of bimodal cells in a fluid layer heated from below with rigid boundaries is studied through numerical computations for Prandtl numbers in the range $10 \lesssim P \lesssim 100$. The stability of the steady solutions with respect to disturbances of various symmetries has been analysed. Typically, the range of stable steady bimodal convection is restricted by the transition to oscillatory bimodal convection. The oscillations preserve the spatial symmetry of the steady bimodal convection pattern in the case of high P and higher wavenumbers, but break it in the case of lower P or lower wavenumbers in the range that has been investigated. Some comparisons are made with experimental observations. The transition from bimodal to knot convection has also been studied.

1. Introduction

The subject of the transition to time dependence in the thermal convection of a high-Prandtl-number fluid has long been a controversial one. Because the inertial terms in the equations of motion become unimportant for sufficiently high Prandtl numbers, the time derivative and advection term in the heat equation become the only source of time dependence and nonlinearity, respectively, in the basic equations of the problem. Laboratory experiments and numerical simulations of two-dimensional (Hansen & Ebel 1988) and three-dimensional convection (Houseman 1988) have demonstrated, however, that the reduced number of degrees of freedom for oscillatory modes is still sufficient to permit the transition to time-dependent convection in a fluid of very large or infinite Prandtl number P. The laboratory evidence is somewhat ambiguous. In her experiments with fluids of different Prandtl numbers Krishnamurti (1970) finds that the Rayleigh number R_{III} for the onset of time dependence in thermal convection becomes essentially independent of P once P exceeds a value of about 50. This value of R_{III} was determined by Krishnamurti to be about 5.3×10^4. On the other hand, Busse & Whitehead (1974, referred to as BW74 in the following), and Whitehead & Parsons (1978) observed steady bimodal convection at Rayleigh numbers far about this value. The steady convection cells in these experiments were realized, however, through the use of two-dimensional rolls as initial conditions at low Rayleigh numbers. In the experiments of Whitehead & Parsons with controlled initial conditions it was possible to observe steady bimodal convection in a fluid with $P = 8600$ up to Rayleigh numbers of the order 8×10^5.

In experiments starting from uncontrolled initial conditions it is difficult to realize the spatially periodic bimodal cells that were achieved in good approximation in the work of BW74, Busse & Whitehead (1971), and Whitehead & Parsons (1978). The basin of attraction of the spatially periodic solutions is rather small in the large-aspect-ratio layers used in the experiments and a random pattern of convection cells is typically found if no special initial conditions are used. Whitehead & Parsons

investigated the question of the onset of oscillations in the random pattern and found that the number of cells exhibiting oscillations increases from a small fraction at a Rayleigh number of the order 10^5 to a majority of the cells at a Rayleigh number of 8×10^5 for $P=8600$. Whitehead & Chan (1976) did similar measurements at lower Prandtl numbers. Clearly the onset of oscillatory time dependence in convection of high-Prandtl-number fluids is not well defined and isolated oscillations will occur first in special locations where strong distortions from the average pattern of bimodal convection cells occur.

In the present paper the dependence of the onset of oscillatory instability of steady bimodal convection on the Prandtl number and on the wavenumbers of the bimodal cells is analysed. It will be demonstrated that the latter dependence is rather strong, which emphasizes the point that variations in the size of the cells may easily give rise to the onset of local oscillations.

The mathematical formulation of the problem in §2 is kept short since the analysis follows earlier work by the authors on three-dimensional convection. In §3 the properties of three-dimensional convection are discussed and compared with those of two-dimensional rolls. The stability of bimodal convection is analysed in §4 and the evolution of the two kinds of oscillatory instability is followed to finite amplitudes in §5. The transition from bimodal convection to knot convection is of particular interest since it involves a change in the wavelength of the pattern. In §6 a few examples of this transition are discussed. The paper closes with some concluding remarks in §7.

2. Mathematical formulation of the problem

We consider a horizontal fluid layer of thickness d with no-slip upper and lower boundaries that are kept at constant temperatures T_1 and T_2, respectively. Using d as lengthscale, d^2/κ as timescale where κ is the thermal diffusivity, and $(T_2-T_1)/R$ as temperature scale we can cast the basic equations in dimensionless form. Since we assume the Boussinesq approximation the velocity field is solenoidal and the following general representation can be employed:

$$\boldsymbol{v}=\boldsymbol{\nabla}\times(\boldsymbol{\nabla}\times\boldsymbol{k}\phi)+\boldsymbol{\nabla}\times\boldsymbol{k}\psi\equiv\boldsymbol{\delta}\phi+\boldsymbol{\varepsilon}\psi, \tag{2.1}$$

where the unit vector $\boldsymbol{k}$ is directed opposite to gravity and parallel to the z-axis of a Cartesian system of coordinates. By taking the z-components of the (curl)^2 and the curl of the equations of motion we obtain the following equations for ϕ and ψ:

$$\nabla^4\Delta_2\phi-\Delta_2\theta=P^{-1}\left\{\boldsymbol{\delta}\cdot[(\boldsymbol{\delta}\phi+\boldsymbol{\varepsilon}\psi)\cdot\boldsymbol{\nabla}(\boldsymbol{\delta}\phi+\boldsymbol{\varepsilon}\psi)]+\frac{\partial}{\partial t}\nabla^2\Delta_2\phi\right\}, \tag{2.2a}$$

$$\nabla^2\Delta_2\psi=P^{-1}\left\{\boldsymbol{\varepsilon}\cdot[(\boldsymbol{\delta}\phi+\boldsymbol{\varepsilon}\psi)\cdot\boldsymbol{\nabla}(\boldsymbol{\delta}\phi+\boldsymbol{\varepsilon}\psi)]+\frac{\partial}{\partial t}\Delta_2\psi\right\}, \tag{2.2b}$$

where Δ_2 denotes the horizontal Laplacian, $\Delta_2\equiv\partial^2/\partial x^2+\partial^2/\partial y^2$. The heat equation for the deviation θ of the temperature from the solution of the static state is given by

$$\nabla^2\theta-R\Delta_2\phi=(\boldsymbol{\delta}\phi+\boldsymbol{\varepsilon}\psi)\cdot\boldsymbol{\nabla}\theta+\frac{\partial}{\partial t}\theta. \tag{2.2c}$$

The Rayleigh and Prandtl numbers obey their usual definitions

$$R\equiv\frac{\gamma g(T_2-T_1)d^3}{\nu\kappa},\quad P\equiv\frac{\nu}{\kappa},$$

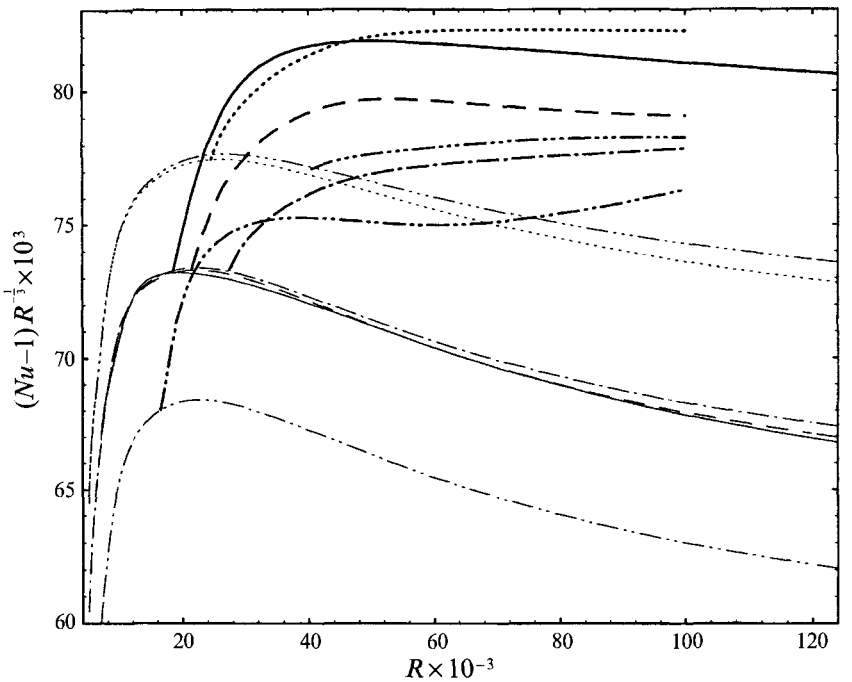

FIGURE 1. Nusselt number Nu as a function of the Rayleigh number R for two-dimensional convection (thin lines) and bifurcating bimodal cells (thick lines). The cases $P = 16$ with $\alpha_y = 2.5$ (dash-dotted), $\alpha_y = 2.0$ (dash-double dotted), $\alpha_y = 3.117$ (dash-triple dotted); $P = 30$ with $\alpha_y = 2.5$ (dashed); $P = 60$ with $\alpha_y = 2.5$ (solid); and $P = 100$ with $\alpha_y = 3.117$ (dotted) have been plotted. $\alpha_x = 4.5$ was used for all bimodal solutions.

where γ is the thermal expansivity, g is the acceleration due to gravity and ν is the kinematic viscosity. The boundary conditions are given by

$$\phi = \frac{\partial}{\partial z}\phi = \psi = \theta = 0 \quad \text{at} \quad z = \pm\tfrac{1}{2}. \tag{2.3}$$

As in previous work on steady bimodal convection at infinite Prandtl number (Frick, Busse & Clever 1983) we use the Galerkin method for the solution of the problem described by equations (2.2) and conditions (2.3). Accordingly the dependent variables are expanded in complete series of functions satisfying the boundary conditions

$$\phi = \sum_{l,m,n} (\hat{a}_{lmn}(t)\cos l\alpha_x x + \check{a}_{lmn}(t)\sin l\alpha_x x)\cos(m\alpha_y y)\, g_n(z), \tag{2.4a}$$

$$\psi = \sum_{l,m,n} (\hat{c}_{lmn}(t)\sin l\alpha_x x + \check{c}_{lmn}(t)\cos l\alpha_x x)\sin(m\alpha_y y)\sin n\pi(z+\tfrac{1}{2}), \tag{2.4b}$$

$$\theta = \sum_{l,m,n} (\hat{b}_{lmn}(t)\cos l\alpha_x x + \check{b}_{lmn}(t)\sin l\alpha_x x)\cos(m\alpha_y y)\sin n\pi(z+\tfrac{1}{2}), \tag{2.4c}$$

where $g_n(z)$ are the Chandrasekhar functions used by Frick *et al.* (1983) and by Clever & Busse (1989). The expansion of the x, y-dependence has been written in the most general form that will be used in the following analysis. For steady bimodal convection a much simpler subset of the representation (2.4) can be used in that

$$\check{a}_{lmn} = \check{b}_{lmn} = \check{c}_{lmn} = 0 \quad \text{for all} \quad l,m,n \tag{2.5a}$$

can be assumed because bimodal cells are characterized by two orthogonal sets of

vertical symmetry planes that can be placed at $x = l\pi/\alpha_x$ and $y = m\pi/\alpha_y$ for all integers l, m. In addition the symmetry property

$$\hat{a}_{lmn} = \hat{b}_{lmn} = \hat{c}_{lmn} = 0 \quad \text{for} \quad l+m+n = \text{odd} \tag{2.5b}$$

is satisfied for steady bimodal convection (Frick *et al.* 1983). The equations for the coefficients $\hat{a}_{lmn}, \hat{b}_{lmn}$, etc. are generated when (2.2) are multiplied by the expansion functions and averaged over the fluid layer after the expansions (2.4) have been inserted for the dependent variables. In the case of steady solutions the resulting nonlinear algebraic equations for the time-independent coefficients can be solved by a Newton–Raphson iteration method once the system of equations has been truncated. We shall neglect for this purpose all coefficients and corresponding equations satisfying

$$l+m+n > N_T, \tag{2.6}$$

where N_T is an integer of the order 10 which can be varied. When sensitive quantities such as the Nusselt number change by less than about 1 % after N_T has been replaced by N_T-2 the approximation is regarded satisfactory. In the case of time-dependent coefficients $\hat{a}_{lmn}, \check{a}_{lmn}$ etc. the algebraic equations are replaced by ordinary first-order differential equations in time. After employing a truncation condition of the form (2.6) we solve the system of equations numerically with the Crank–Nicolson integration scheme. Because of the higher computational expense for time-dependent solutions a slightly less restrictive truncation criterion than for the steady solutions is usually applied.

The stability of the steady bimodal convection flow can be analysed through the imposition of infinitesimal disturbances of the following general form:

$$\tilde{\phi} = \sum_{l,m,n} \tilde{a}_{lmn} \exp\{\mathrm{i}(l\alpha_x + d)\, x + \mathrm{i}(m\alpha_y + b)\, y + \sigma t\}\, g_n(z), \tag{2.7a}$$

$$\tilde{\psi} = \mathrm{i} \sum_{l,m,n} \tilde{c}_{lmn} \exp\{\mathrm{i}(l\alpha_x + d)\, x + \mathrm{i}(m\alpha_y + b)\, y + \sigma t\} \sin n\pi(z+\tfrac{1}{2}), \tag{2.7b}$$

$$\tilde{\theta} = \sum_{l,m,n} \tilde{b}_{lmn} \exp\{\mathrm{i}(l\alpha_x + d)\, x + \mathrm{i}(m\alpha_y + b)\, y + \sigma t\} \sin n\pi(z+\tfrac{1}{2}). \tag{2.7c}$$

For a given steady solution characterized by the parameters R, P, α_x and α_y the equations for the disturbances $\tilde{\phi}, \tilde{\psi}, \tilde{\theta}$ represent an eigenvalue problem with the growth rate σ as eigenvalue. When the maximum of the real part of σ as a function of d and b exceeds zero, the steady solution becomes unstable. Since the summation in (2.7) runs through negative as well as positive integers l and m, the general eigenvalue problem involves about four times as many equations as the problem for the steady solution after the truncation condition (2.6) has been imposed for $|l|$ and $|m|$ instead of l and m. Fortunately, the strongest growing disturbances often correspond to $d = b = 0$, in which case reductions in the size of the stability matrix become possible as will be discussed in §4.

3. Properties of steady bimodal convection

It is well known that the transition from rolls to bimodal convection arises from the instability of the thermal boundary layers at the rigid upper and lower boundaries of the fluid layer (Busse 1967). The additional small-wavelength convection roll that develops at a right angle to the basic roll is particularly suited to take advantage of the buoyancy stored in the thermal boundary layers. In conjunction with the release of buoyancy the heat transport is increased as shown for a variety of cases in figure 1. This figure clearly shows the striking increase of the Nusselt number due to the onset of

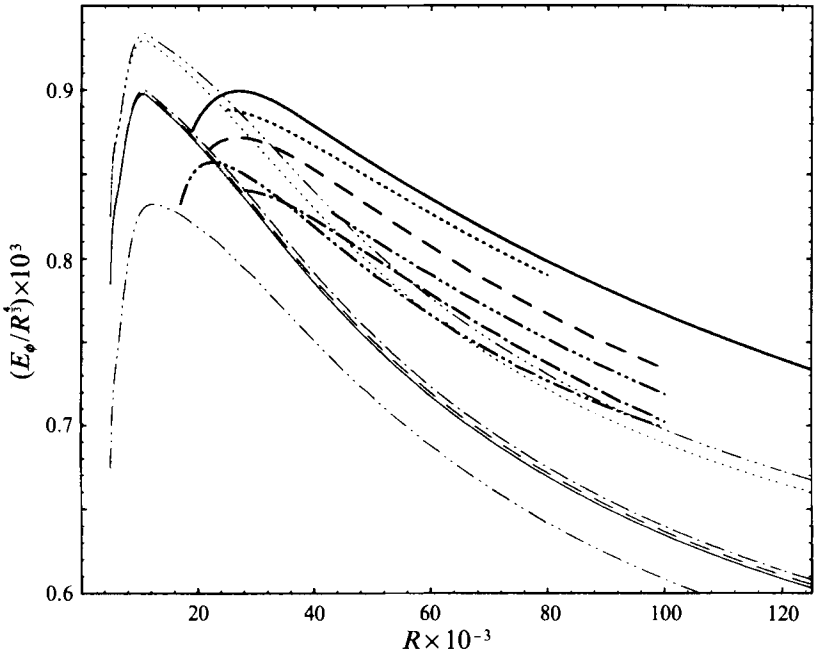

FIGURE 2. The kinetic energy E_ϕ for the poloidal component of motion as a function of R for the same cases as in figure 1.

bimodal convection. Without this onset the Nusselt number would asymptotically follow the $R^{\frac{1}{3}}$-law that has been predicted for two-dimensional rolls (Roberts 1979). While the heat transport of two-dimensional convection depends strongly on the wavenumber α_y of the primary rolls and only slightly on the Prandtl number, the wavenumber dependence is reduced after the onset of bimodal convection in that the second roll component tends to compensate somewhat for the deficiency of the primary roll component. On the other hand a more substantial Prandtl-number dependence seems to develop in that the contribution of the secondary roll component is especially strong at higher Prandtl numbers.

The poloidal and toroidal kinetic energies of motion are defined by

$$E_\phi \equiv \tfrac{1}{2}\langle|\nabla\times(\nabla\times\boldsymbol{k}\phi)|^2\rangle, \quad E_\psi \equiv \tfrac{1}{2}\langle|\nabla\times\boldsymbol{k}\psi|^2\rangle, \tag{3.1}$$

where the angular brackets indicate the average over the fluid layer. Their dependences on the Rayleigh number are shown in figures 2 and 3 for the same parameters as in figure 1. The poloidal kinetic energy E_ϕ exhibits a dependence similar to that of the Nusselt number while the toroidal energy E_ψ vanishes for the two-dimensional rolls and remains relatively small for bimodal convection. As expected, E_ϕ decreases with increasing Prandtl number, but the dependence on α_y is even more pronounced in that long wavelengths promote the generation of vertical vorticity in bimodal convection. The choice of the wavenumbers α_x has been motivated in part by the preferred values determined in the stability analysis of Busse (1967) and Bolton, Busse & Clever (1986).

The structure of velocity and temperature fields of steady bimodal convection appear to change little with Prandtl number. The variation with Rayleigh number is much stronger as is evident from figure 4 where cases with $R = 2.8\times 10^4$ and 10^5 are compared. While the structure of the basic roll is still quite apparent at the lower Rayleigh number, a rectangular cell is evident at $R \approx 10^5$. For plots of isotherms in the vertical planes we refer to the computations of Frick *et al.* (1983) of bimodal

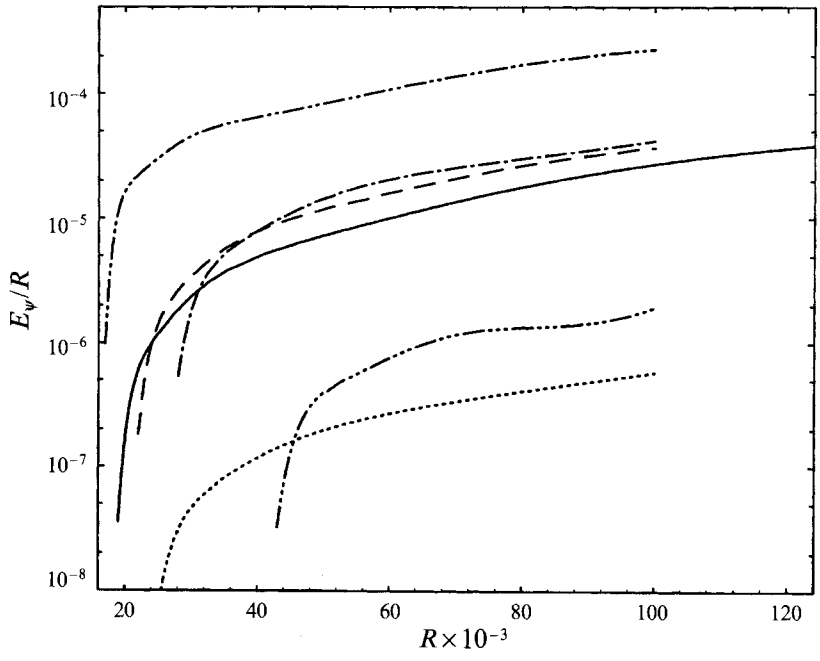

FIGURE 3. The kinetic energy E_ψ for the toroidal component of motion in bimodal cells for the same cases as in figure 1.

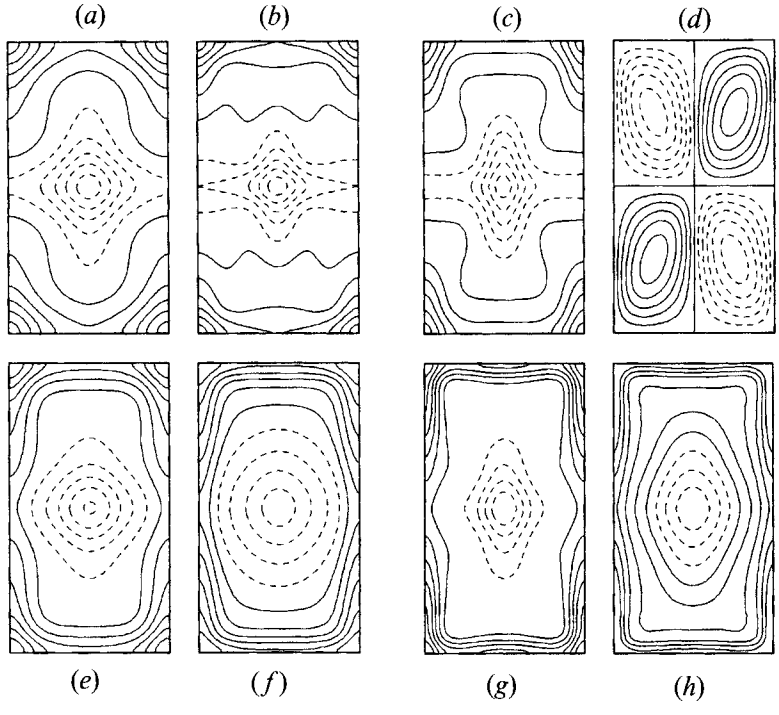

FIGURE 4. Lines of constant vertical velocity in the planes $z = 0$ (a, c) and $z = -0.4$ (e, g), isotherms in the planes $z = 0$ (b) and $z = -0.4$ (f, h) and lines of constant ψ in the plane $z = 0$ (d). The left (right) half of the figure correspond to the parameter values $P = 100$ (60), $R = 2.8 \times 10^4$ (1×10^5) with $\alpha_x = 4.5$, $\alpha_y = 2.5$ in all cases. Solid (dashed) lines indicate positive (negative) values except for the solid line adjacent the dashed lines which indicates zero

convection at infinite Prandtl numbers. It should be noted that the missing parameter values in the caption of figure 3 in that paper are given by $\alpha_1 = 3.117$, $\alpha_2 = 5.0$ and $R = 3 \times 10^4$. It is clear from the smaller values of E_ψ that the qualitative difference of the solutions at infinite and at finite Prandtl numbers arising from the presence of vertical vorticity in the latter case does not cause a significant change in the gross structures of the solutions.

4. Transition to oscillatory bimodal convection

The stability of steady bimodal convection has been analysed with respect to disturbances which fit the horizontal periodicity interval defined by α_x, α_y. These disturbances usually appear to be the most dangerous ones according to the experimental evidence of BW74. Because of the symmetry properties (2.5) the disturbances of the form (2.7) with $b = d = 0$ can be separated into different subsets depending on whether they possess the same symmetry or the opposite one as the steady solution. Accordingly we may separate the disturbances into two sets with respect to the x-dependence,

$$(C) \text{ with } \tilde{a}_{lmn} = \tilde{a}_{-lmn} \quad \text{and} \quad (S) \text{ with } \tilde{a}_{lmn} = -\tilde{a}_{-lmn}, \tag{4.1}$$

and an analogous separation for the y-dependence. The same relationships hold for the coefficient $\tilde{b}_{lmn}$ and $\tilde{c}_{lmn}$. In addition we separate the disturbances into sets for which the coefficients $\tilde{a}_{lmn}, \tilde{b}_{lmn}, \tilde{c}_{lmn}$ vanish unless $l+m+n$ is even (denoted by E) and those for which coefficients vanish unless $l+m+n$ is odd (denoted by O). We thus find eight subsets of disturbances:

$$ECC, ECS, ESC, ECC, OCC, OCS, OSC, OSS. \tag{4.2}$$

$C(S)$ as second or third letter indicates a cosine (sine) dependence of $\tilde{\phi}$ with respect to the x- or the y-coordinate, respectively.

The separation of the general stability matrix into the subsets (4.2) yields an enormous simplification of the eigenvalue problem for the determination of the growth rates σ. The critical values R_{III} of the Rayleigh number at which the maximum real part of σ goes through zero have been listed in table 1 for typical steady bimodal solutions, together with the symmetry of the growing disturbances. It is evident from this table that for Prandtl numbers less than 60, disturbances with the OSC-symmetry are the critical ones while for larger Prandtl numbers disturbances with the ECC-symmetry also enter the competition. There is a significant dependence on the wavenumbers of the steady bimodal cells. Smaller bimodal cells, especially those with higher wavenumber α_x, appear to be much more stable than those with lesser values of α_x which is in qualitative agreement with the results of figure 5 in BW74.

The measured Rayleigh numbers for the onset of oscillatory instability appear to be too high by a factor of at least two when compared with the values listed in table 1. This discrepancy must be attributed in part to the effect of the finitely conducting boundaries of the experimental layer which also tends to shift the preferred wavenumbers towards lower values (Busse & Whitehead 1971). Another cause for the discrepancy arises from the transient nature of the experiments. Instabilities are observed only when they grow sufficiently fast, which happens usually only at a considerable distance beyond the computed stability boundary.

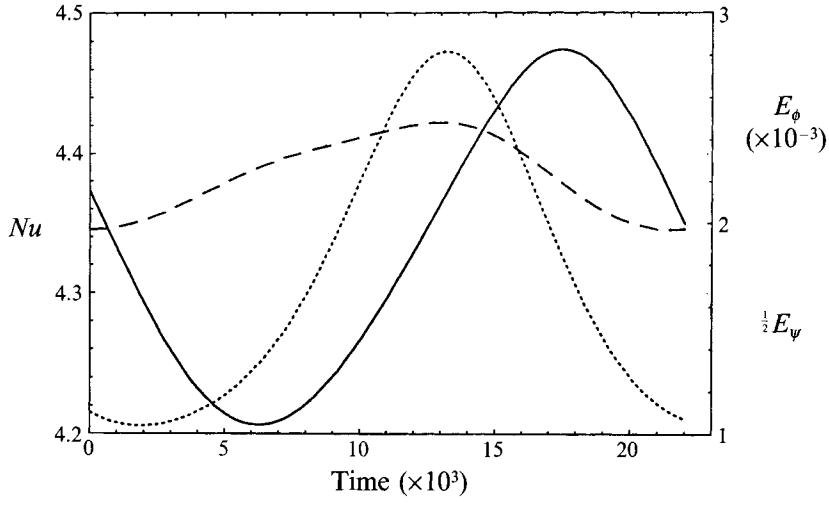

FIGURE 5. Variation in time t of Nusselt number Nu (solid line, left ordinate), poloidal kinetic energy E_ϕ (dashed, right ordinate) and toroidal kinetic energy E_ψ (dotted, right ordinate) of wavy oscillatory bimodal convection for the case $P = 16$, $R = 7 \times 10^4$, $\alpha_x = 4.5$, $\alpha_y = 2.5$.

P	α_x	α_y	$R_{III} \times 10^{-3}$	σ_i	Symmetry
16	4.5	2.0	38.8	89.1	*OSC*
	4.5	2.5	35.6	106.1	*OSC*
	4.5	3.117	59.7	167.5	*OSC*
	5.4	2.5	83.6	152.9	*OSC*
30	4.5	2.5	55.1	125.1	*OSC*
	4.5	3.117	69.3	174.4	*OSC*
60	3.6	2.0	39.7	92.2	*OSC*
	4.5	2.0	74.7	184.3	*ECC*
	3.6	2.5	37.0	114.1	*OSC*
	4.0	2.5	40.4	114.3	*OSC*
	4.5	2.5	109.0	226.8	*ECC*
	5.4	2.5	> 250		
	4.5	3.117	80.7	182.4	*OSC*
	5.4	3.117	> 250		
100	4.5	3.117	96.6	195.2	*OSC*

TABLE 1. Onset of oscillatory instability of bimodal convection

5. Wavy and symmetric oscillatory bimodal convection

In this section we describe results obtained for oscillatory bimodal convection at finite amplitudes of the oscillatory component. In contrast of the linear analysis of the preceding section based on the representation (2.7) we now use the method of forward integration in time of the equations for the time-dependent coefficients in the representation (2.4). The wavy oscillatory bimodal convection evolving from the *OSC*-disturbances usually causes much stronger deviations from the steady bimodal flow than the symmetric oscillatory bimodal convection evolving from the *ECC*-disturbances. In figure 5 the variation in time of integral properties such as the Nusselt number Nu and the kinetic energies E_ϕ and E_ψ is shown. The latter energies are out of phase with the Nusselt number in that their maxima precede that of Nu by about 90°.

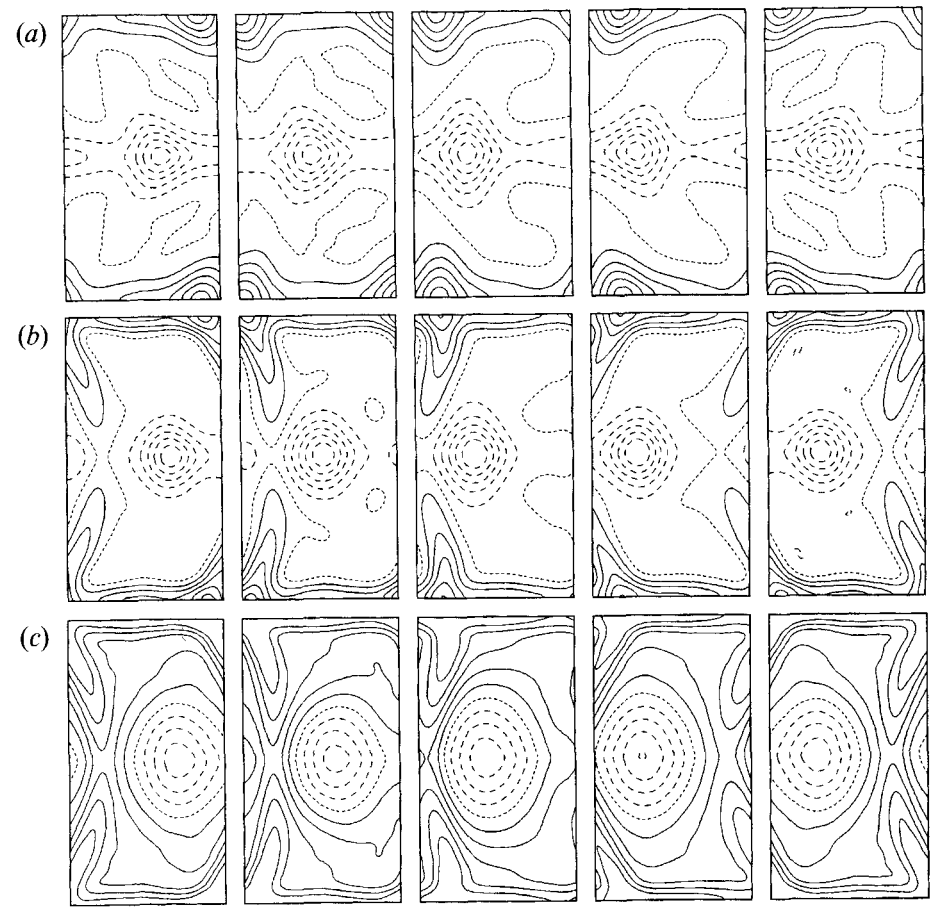

FIGURE 6. Lines of constant vertical velocity in planes $z = 0$ (row *a*) and $z = -0.4$ (row *b*) and of isotherms in the plane $z = -0.4$ (row *c*) at the times (left to right) $t = 0$, 5.5×10^{-3}, 11.0×10^{-3}, 16.5×10^{-3}, 22×10^{-3} of figure 5, such that each row of five pictures shows about one half-period of oscillations. Solid (dashed) lines indicate positive (negative) values; the short-dashed line indicates zero. Parameter values are the same as in figure 5.

The period of integral properties actually corresponds to one half-period of the pattern oscillations as is evident from the comparison with figures 6–8. The waving back and forth of the rising and descending sheets of the secondary rolls seen in figure 6 is typical for wavy oscillatory bimodal convection. This phenomenon is also clearly apparent in the isotherms of the vertical planes $y = 0$, $y = \pi/2\alpha_y$, and $y = \pi/\alpha_y$ shown in figure 7. In figure 8 it is shown that the variation in the Nusselt number corresponds to the rise of hot fluid blobs towards the cold boundary and their subsequent dissipation there as seen in columns (*a*) and (*d*) of the figure. The corresponding movement of cold blobs is seen in plane $x = \pi/\alpha_x$ (column *c*) where the dashed isotherms form a mirror image of the solid isotherms in the plane $x = 0$.

The period of integral properties of symmetric oscillatory bimodal convection is identical to the period exhibited by the local properties, in contrast to the case of wavy oscillatory bimodal convection. This result is a consequence of the fact that the spatial symmetry of the bimodal cells is not broken by the onset of symmetric oscillations. Figure 9 indicates a relative slight variation of Nu and E_ϕ even though the critical Rayleigh number for the onset of oscillations has been exceeded by 28 %. Note that Nu,

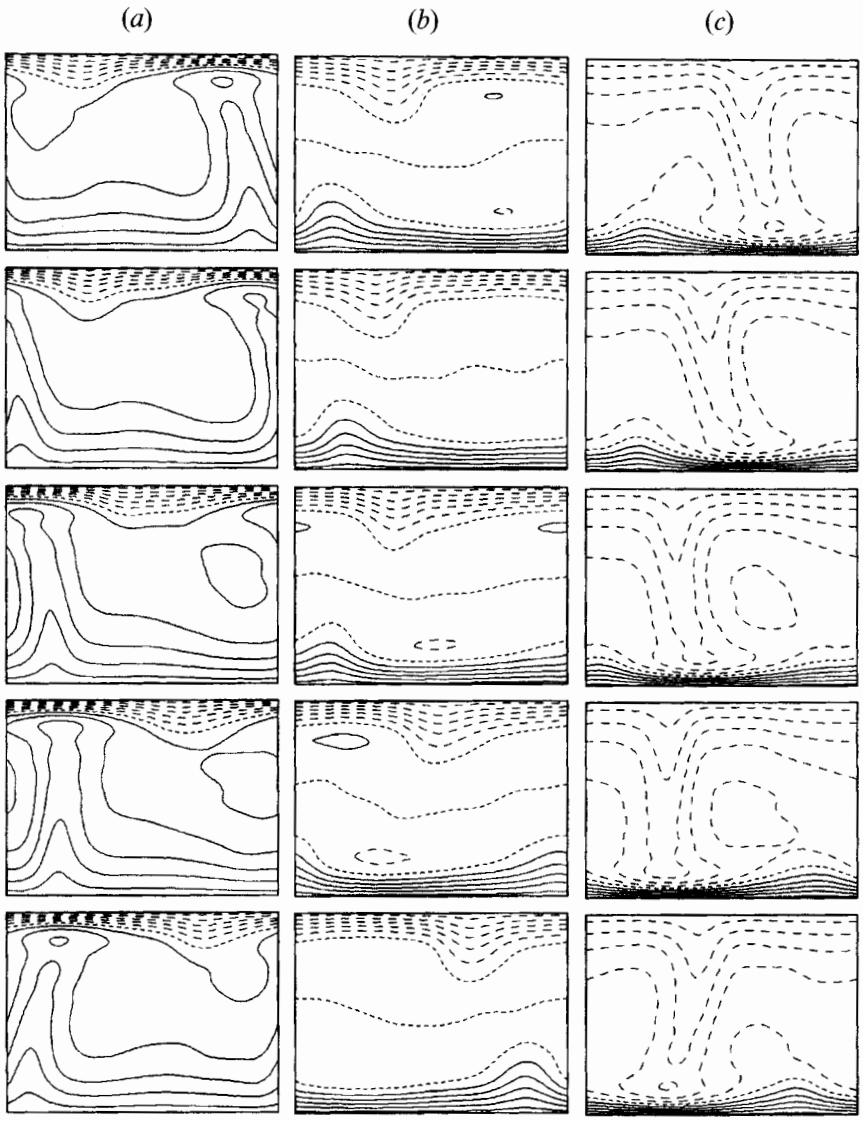

FIGURE 7. Isotherms in the planes $y = 0$ (column a), $y = \pi/2\alpha_y$ (column b) and $u = \pi/\alpha_y$ (column c) for the same case as in figure 6. Time increases from top to bottom.

E_ϕ and E_ψ are varying nearly in phase. The variations of velocity and temperature fields throughout the cycle are shown in figures 10 and 11. They are best seen near the thermal boundary layers where regions of hot rising fluid and cold descending fluid, respectively, expand and contract in a periodic fashion. The computed features of both wavy and symmetric oscillatory bimodal convection agree well with the observations reported in BW74. Figures 2 and 7 of that paper show the waving back and forth of rising sheets of the secondary roll motion while the expansion and contraction of these sheets in the form of the symmetric oscillatory bimodal convection occurs in the case of a higher wavenumber α_x as shown in figure 9 of that paper. Both types of oscillatory bimodal convection are associated with a higher time-averaged heat transport than is carried by steady bimodal cells for the same parameter values. As the Rayleigh number increases this difference tends to decrease and sometimes it reverses its sign, as

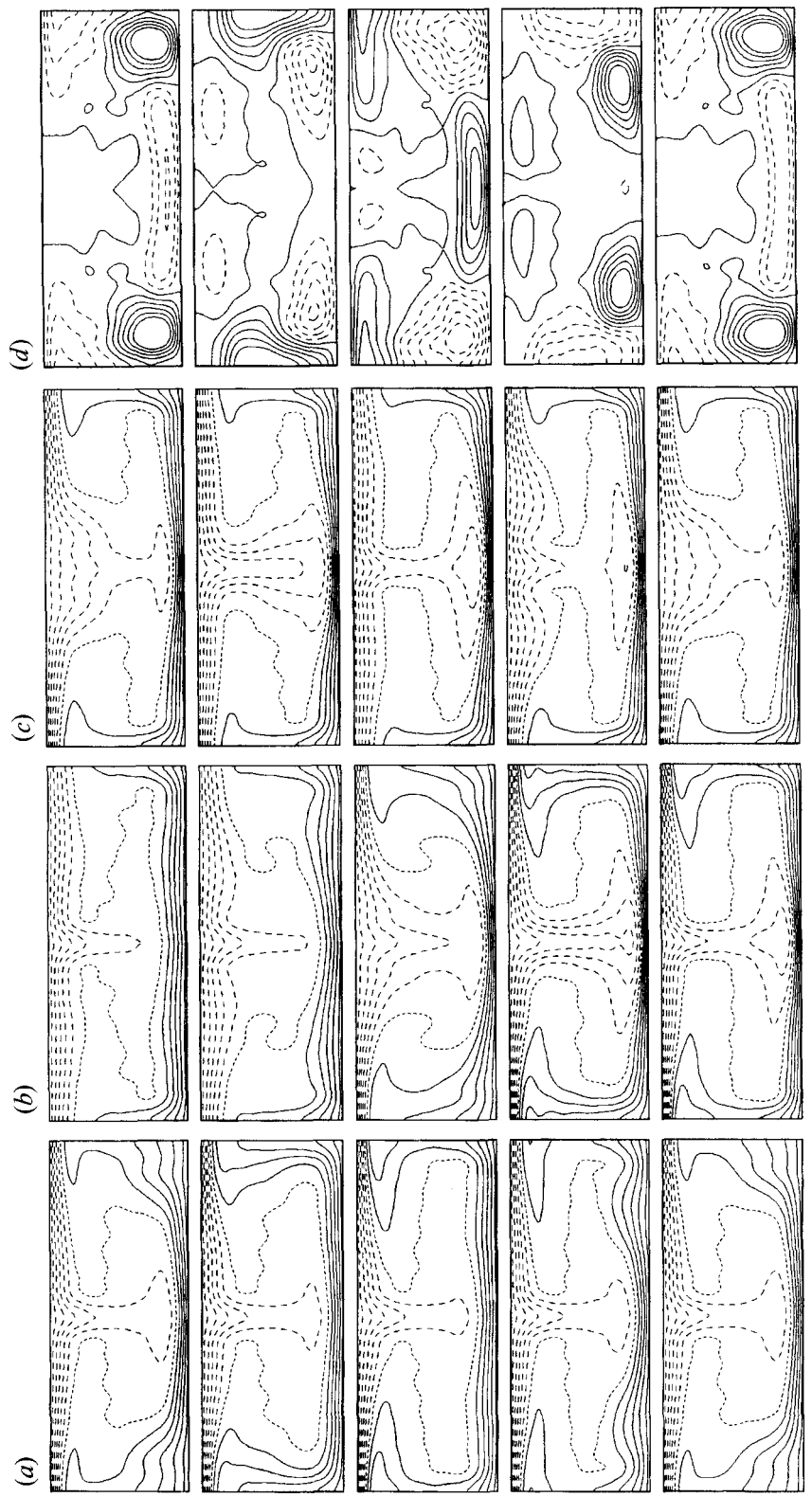

FIGURE 8. Isotherms in the plane $x = 0$ (column *a*), $x = \pi/2\alpha_x$ (column *b*), $x = \pi/\alpha_x$ (column *c*) and deviations of the isotherms from their time average in the plane $x = 0$ (column *d*) for the same case as in figure 6. Time increases from top to bottom.

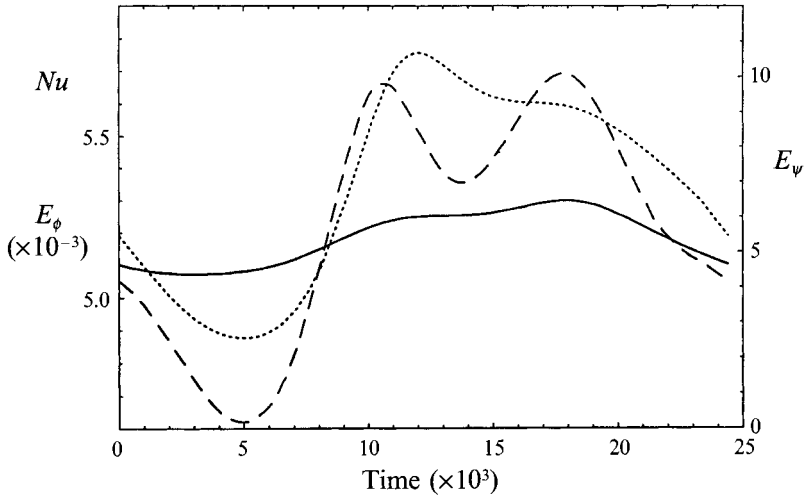

FIGURE 9. Variation in time t of the Nusselt number Nu (solid line, left ordinate), E_ϕ (dashed, left ordinate) and E_ψ (dotted, right ordinate) of symmetric oscillatory bimodal convection for the case $P = 60$, $R = 14 \times 10^4$, $\alpha_x = 4.5$, $\alpha_y = 2.5$. $N_T = 16$ has been used as truncation.

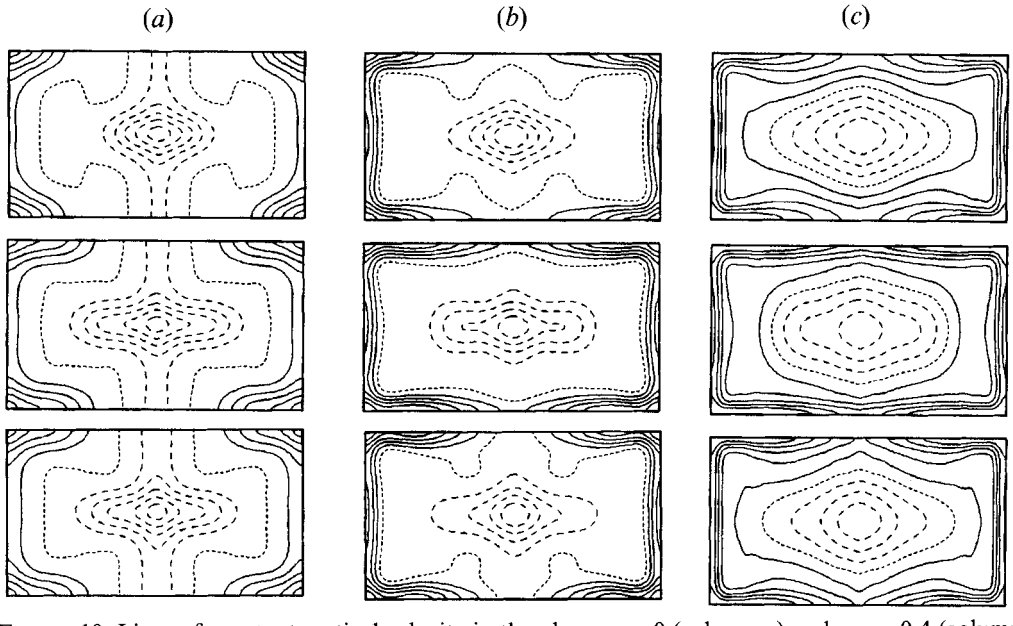

FIGURE 10. Lines of constant vertical velocity in the planes $z = 0$ (column a) and $z = -0.4$ (column b) and isotherms in the plane $z = -0.4$ (column c) of symmetric oscillatory bimodal convection for the case of figure 9 at the times (top to bottom) $t = 4 \times 10^{-3}$, 12×10^{-3}, 20×10^{-3} such that the picture at $t = 28 \times 10^{-3}$ would be nearly the same as the first one.

indicated in table 2. In this comparison it must be taken into account that a lower truncation parameter had to be used for wavy oscillatory solutions because of the high expense for the computations of time-dependent solutions with a broken symmetry. Although the variation of the Nusselt number with the truncation parameter N_T is still larger than the difference between oscillatory and steady cases, the above statements are justified. The variation with N_T is a systematic one and differences for a given value of N_T tend to persist as N_T is increased.

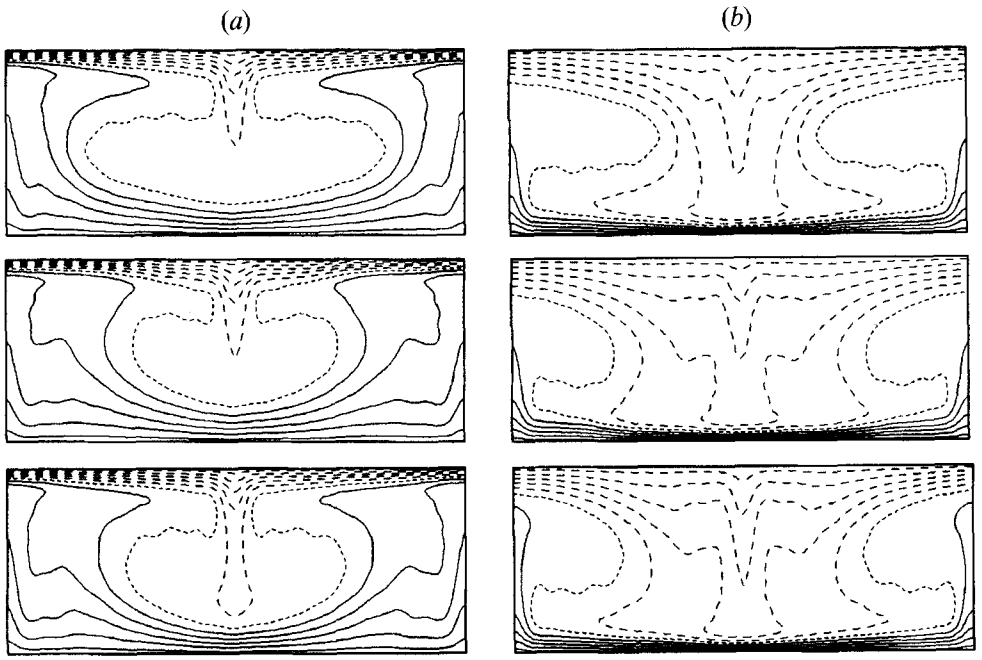

FIGURE 11. Isotherms in the planes $x = 0$ (*a*) and $x = \pi/\alpha_x$ (*b*) for the same case as figure 10.

							Nu for steady case		
P	α_x	α_y	$R \times 10^{-3}$	Period $\times 10^3$	N_T	Nu	$N_T = 12$	$N_T = 14$	$N_T = 16$
16	4.5	2.5	50	50.2	12	3.917	3.871	3.845	3.833
			70	43.3	12	4.333	4.257	4.214	4.191
16	4.5	2.0	50	60.8	12	3.825	3.803	3.777	3.765
			70	51.2	12	4.161	4.164	4.119	4.096
30	4.5	2.5	70	44.2	12	4.348	4.328	4.290	4.270
			100	37.0	12	4.767	4.768	4.705	4.671
60	4.5	2.5	120	26.4	16	4.986	5.072	5.010	4.982
			140	24.4	16	5.187	—	—	5.172

TABLE 2. Selected time-averaged Nusselt numbers for oscillatory bimodal convection in comparison with values for steady solutions

In figure 12 the periods of oscillatory bimodal convection have been plotted as a function of the Rayleigh number in order to offer a comparison with the corresponding figure 5 of BW74 in which experimental measurements have been plotted. Although theoretical predictions and experimental measurements overlap in a small Rayleigh-number range, the experimental data continue the line of figure 12 towards higher Rayleigh numbers. Both figures exhibit the general $R^{-\frac{2}{3}}$-dependence proposed by Howard (1966) in his model of periodic eruptions of thermals from the thermal boundary layers. Experimentally the $R^{-\frac{2}{3}}$-dependence was found by Rossby (1969). The property that the period of oscillations is independent of the Prandtl number indicates a connection with the circulation velocity of the basic roll, which also grows with nearly the $R^{\frac{2}{3}}$-power as shown in figure 2. Indeed, the oscillations may be regarded as a resonance phenomenon in which half a circulation period matches approximately the timescale for the growth and subsequent instability of the thermal boundary layers,

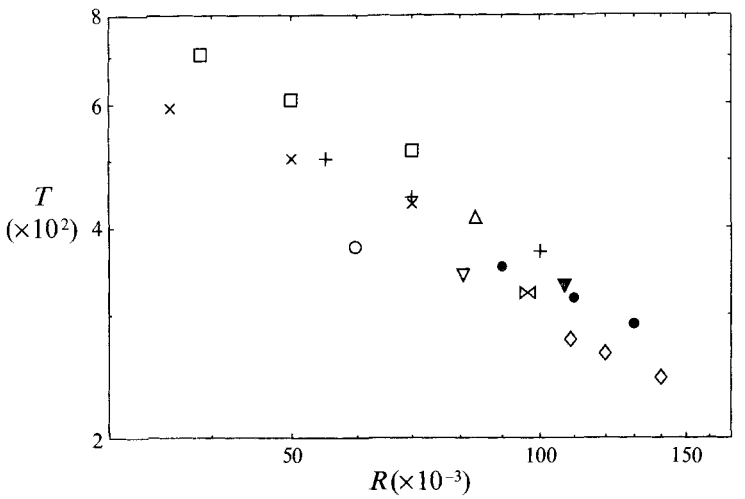

FIGURE 12. Periods of T of oscillatory bimodal convection as a function of R. Parameter values (P, α_x, α_y) are ×, 16, 4.5, 2.0; □, 16, 4.5, 2.5; +, 30, 4.5, 2.5; △, 16, 5.4, 2.5; ◇, 60, 4.5, 2.5; ○, 16, 4.5, 3.117; ▽, 60, 4.5, 3.117; ⋈, 100, 4.5, 3.117. For comparison some data points from figure 5 of BW74 have also been plotted: ●, $P = 63$; ▼, $P = 44$.

since two hot and cold blobs appear to move around the convection cell at any time. The role of the circulation velocity is also indicated by the fact that the roll velocity field depends much more on the wavenumber α_y than on the Prandtl number as is evident from figure 2. Both experimental as well as theoretical results exhibit the expected property that the period of oscillation increases with decreasing α_y.

6. Transition from bimodal to knot convection

Knot convection and bimodal convection exhibit a number of similarities. Both types of convection in their steady form share the symmetry properties (2.5) for the representation (2.4). Even in their oscillatory forms they are rather similar in that the emergence of hot and cold blobs from the hot and cold boundary layers, respectively, is the dominant mechanism for the transition from steady to oscillatory convection. The main difference is the property that for bimodal convection the secondary wavenumber α_x is significantly larger than the critical value α_c while the opposite holds for knot convection.

Bimodal convection is the preferred tertiary state of convection at high Prandtl numbers and knot convection assumes this role in the range $2 \lesssim P \lesssim P_t$, where P_t increases from about 10 at a Rayleigh number of the order 3×10^4 to much higher values as R increases. The stability boundary at P_t corresponds to the transition from knot convection to bimodal cells and vice versa.

In order to analyse the instability of steady bimodal convection with respect to disturbances which cause a transition to knot convection, infinitesimal perturbations of the form (2.7) must be admitted which change the periodicity interval of bimodal cells. Since the wavenumbers α_x for bimodal and knot convection differ typically by a factor of three, we have found it convenient to replace the value α_x in the representation (2.4) for bimodal convection by $\frac{1}{3}\alpha_x$ such that only those coefficients a_{lmn} for which $l = 3p$ for $p = 0, 1, 2, \ldots$ are different from zero. Within this new enlarged representation, disturbances of the form (2.7) which increase the wavelength of

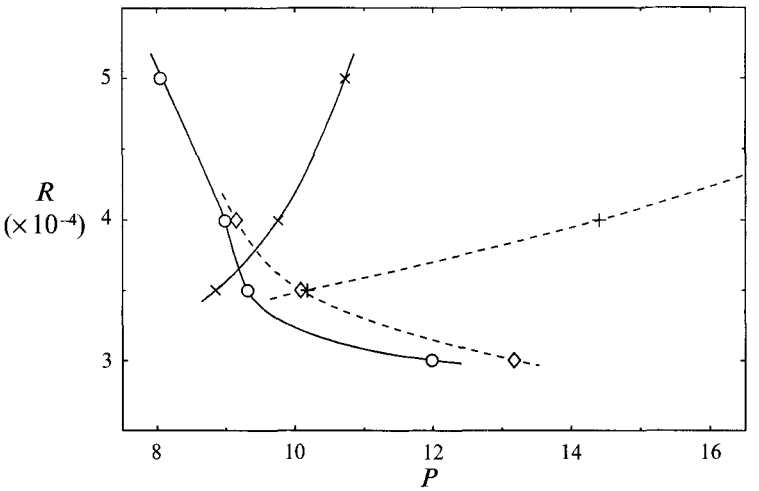

FIGURE 13. Stability boundaries as a function of R and P of steady bimodal convection with $\alpha_x = 5.4$, $\alpha_y = 2.5$ (solid lines), and with $\alpha_x = 4.5$, $\alpha_y = 2.5$ (dashed lines) with respect to the transition to steady knot solutions with $\tilde{\alpha}_x = \frac{1}{3}\alpha_x$ ($\diamond$, $\bigcirc$) and with respect to the transition to oscillatory knot convection with $\tilde{\alpha}_x = \frac{1}{3}\alpha_x$ ($\times$, $+$).

bimodal cells in the x-direction by a factor of three can be accommodated still with vanishing values of d and b. Figure 13 shows some results of this stability analysis for two different periodicity intervals of the bimodal cells. As must be expected the transition to steady knot convection occurs at low Rayleigh numbers while at higher Rayleigh numbers an oscillatory instability is found which evolves into oscillatory knot convection. Obviously it is difficult to do computations in more than a few cases because of the high truncation required. But the results of figure 11 demonstrate a process which resembles closely the transition found in the laboratory experiments of BW74. A quantitative comparison cannot be easily carried out, however, because most of the observations have been done at higher Prandtl and Rayleigh numbers.

7. Concluding remarks

The thermal boundary layers at the top and bottom boundaries are the dominant nonlinear feature in the high-Rayleigh-number high-Prandtl-number convection. The instability of these layers causes both the transition from roll convection to bimodal cells and the emergence of blob instabilities. That the onset of the oscillatory instability is usually delayed when the Nusselt number is high can be seen from a comparison of the results shown in figure 1 and table 1. In the case of the highest heat transport, namely bimodal convection with $\alpha_x = 5.4$, $\alpha_y = 3.117$ in the case $P = 60$, an onset of oscillatory instability could not be found in the range of Rayleigh numbers that has been investigated.

The onset of oscillations is not solely influenced by the thickness of the thermal boundary layers. Relatively low values of α_x also seem to promote the onset of oscillations. Computations in the case $P = 16$, $\alpha_x = 3.5$, $\alpha_y = 4.5$ have given the result that the steady bimodal convection is always unstable to oscillatory instabilities. The sensitive dependence of the oscillatory instabilities on the wavenumbers of the bimodal cells is the reason for the very inhomogeneous onset of oscillations in experiments started without controlled initial conditions. As shown by Whitehead & Chan (1976) and Whitehead & Parsons (1978) the onset of time dependence of convection in high-

Prandtl-number fluids is spread out over a large Rayleigh-number range starting with oscillatory blobs in isolated spots of the convection layer at a relatively low Rayleigh number R_i. As R increases, the oscillatory cells become more numerous. Not until a Rayleigh number of at least twice R_i has been reached does every convection cell participate in the oscillations. This latter Rayleigh number corresponds roughly to the onset of oscillations for periodic bimodal cells with average wavenumbers.

Because of their small basin of attraction in the phase space of the problem, spatially periodic steady and oscillatory bimodal cells are realized experimentally only under special conditions and usually more randomly organized patterns are observed. Nevertheless the regular solutions obtained in this paper can be regarded as representative examples in their respective Rayleigh- and Prandtl-number regimes since they exhibit typical features in their most simple form such as the interaction of steady and fluctuating components of motion. By extending the present analysis to higher Rayleigh numbers or by measuring in more detail experimentally realized spatially periodic convection it should also be possible to reach an even better quantitative comparison between theory and observations than has been obtained so far.

The research reported in this paper has been supported by the Atmospheric Sciences Section of the US National Science Foundation and by a NATO travel grant.

REFERENCES

BOLTON, E. W., BUSSE, F. H. & CLEVER, R. M. 1986 Oscillatory instabilities of convection rolls at intermediate Prandtl numbers. *J. Fluid Mech.* **164**, 469–485.

BUSSE, F. H. 1967 On the stability of two-dimensional convection in a layer heated from below. *J. Math. Phys.* **46**, 140–150.

BUSSE, F. H. & WHITEHEAD, J. A. 1971 Instabilities of convection rolls in a high Prandtl number fluid. *J. Fluid Mech.* **47**, 305–320.

BUSSE, F. H. & WHITEHEAD, J. A. 1974 Oscillatory and collective instabilities in large Prandtl number convection. *J. Fluid Mech.* **66**, 67–79 (referred to herein as BW74).

CLEVER, R. M. & BUSSE, F. H. 1989 Three-dimensional knot convection in a layer heated from below. *J. Fluid Mech.* **198**, 345–363.

FRICK, H., BUSSE, F. H. & CLEVER, R. M. 1983 Steady three-dimensional convection at high Prandtl number. *J. Fluid Mech.* **127**, 141–153.

HANSEN, U. & EBEL, A. 1988 Time-dependent thermal convection – a possible explanation for a multiscale flow in the Earth's mantle. *Geophys. J.* **94**, 181–191.

HOUSEMAN, G. 1988 The dependence of convection planform on mode of heating. *Nature* **332**, 346–349.

HOWARD, L. N. 1966 Convection at high Rayleigh number. In *Proc. 11th Intl. Congr. of Appl. Mech., Munich 1964* (ed. H. Görtler), pp. 1109–1115. Springer.

KRISHNAMURTI, R. 1970 On the transition to turbulent convection. Part 2. The transition to time-dependent flow. *J. Fluid Mech.* **42**, 309–320.

ROBERTS, G. O. 1979 Fast viscous Bénard convection. *Geophys. Astrophys. Fluid Dyn.* **12**, 235–272.

ROSSBY, H. T. 1969 A study of Bénard convection with and without rotation. *J. Fluid Mech.* **36**, 309–335.

WHITEHEAD, J. A. & CHAN, G. L. 1976 Stability of Rayleigh–Bénard convection rolls and bimodal flow at moderate Prandtl number. *Dyn. Atmos. Oceans* **1**, 33–49.

WHITEHEAD, J. A. & PARSONS, B. 1978 Observations of convection at Rayleigh numbers up to 760000 in a fluid with large Prandtl number. *Geophys. Astrophys. Fluid Dyn.* **9**, 201–217.